Angular distributions for two-photon double ionization of lithium

G. S. J. Armstrong and J. Colgan
Theoretical Division, Los Alamos National Laboratory, Los Alamos, New Mexico 87545, USA
(Received 9 June 2012; published 10 August 2012)

We present angular distributions for two-photon double ionization of lithium at photon energies of 50 eV ($\lambda = 25$ nm) and 59 eV ($\lambda = 21$ nm). The results are obtained from full-dimensional solution of the two-active-electron time-dependent Schrödinger equation using the time-dependent close-coupling method. We investigate two different double ionization mechanisms. First, we consider direct double ionization of the Li ground state following the absorption of two photons. Secondly, we consider an initial photoexcitation of the $1s2s2p$ doubly excited state, followed by photoionization of the $2s$ and $2p$ electrons. We find significant differences between the angular distributions obtained for these two distinct processes. We also compare the characteristics of the angular distributions for Li with those of other two-electron atoms.

DOI: 10.1103/PhysRevA.86.023407 PACS number(s): 32.80.Fb, 32.80.Aa

I. INTRODUCTION

The advent of free-electron laser technology has generated significant interest in the study of few-photon reactions at VUV and EUV wavelengths. Pioneering measurements of recoil-ion momentum distributions for two-photon double ionization of lithium are currently under way at the FLASH free-electron laser facility in Hamburg, augmenting previous measurements for helium and neon [1–3]. These experiments are capable of providing electron momentum and angular distributions for few-photon double ionization, thereby complementing the numerous theoretical calculations of such quantities. These techniques have recently been applied to double ionization of lithium at XUV wavelengths [4] and single ionization of lithium at Ti:sapphire wavelengths [5]. Moreover, the physics of atoms exposed to VUV laser wavelengths is quite different from the physics of atoms exposed to infrared light. At the longer infrared wavelengths, the laser field interacts predominantly with outer-shell electrons. At shorter VUV wavelengths, the atomic response is more intricate, with inner-shell processes becoming more significant. Such processes have recently been investigated using R-matrix Floquet techniques, and have demonstrated significant emission of $2s$ electrons in single ionization of Ne^+ [6,7], as well as emission of $1s$ electrons from Li^- [8]. Recently, two-photon double ionization of inner-shell $4d$ electrons in Xe has been observed in experiment [9] and studied in theory [10].

In anticipation of these experiments, much theoretical emphasis over the last decade has been placed on calculating generalized cross sections for two-photon double ionization of helium using a variety of theoretical approaches [11–24]. Despite these efforts, quantitative agreement between the different methods has not yet been reached, and only two experimental data points [25,26] are currently available for comparison. The lack of experimental data is mainly due to the large two-electron ionization potential of He, which leads to low double-ionization rates, which in turn imposes severe vacuum requirements for accurate cross section measurement. However, good agreement has been obtained between a number of recent theoretical studies [21,23,24] and one of the measurements [25].

The two-photon double ionization of helium has naturally received great attention since it represents the simplest two-photon three-body Coulomb problem. Aside from He, the only other two-electron systems for which calculated triple differential cross sections for two-photon double ionization are currently available are H_2 [27–30] and H^- [31]. The lithium atom is the next simplest few-electron system for which *ab initio* theory can provide support for experiment. However, the nature of the Li atom introduces a number of new levels of complexity. First, the $1s^2 2s\ ^2S$ Li ground state allows two electrons from different shells to interact with the laser field. Such interactions have previously been studied by varying the initial state in double photoionization of helium [32]. Striking differences were observed in the total cross section for initial $1s2s\ ^{1,3}S$ metastable states in comparison to those obtained using an initial $1s^2\ ^1S$ ground state. Secondly, since the Li ground state is a doublet state, the two ejected electrons may have either singlet or triplet symmetry.

In this paper, we examine angular distributions of the outgoing electrons following two-photon double ionization of Li at photon energies of 50 and 59 eV. At these two photon energies, double ionization proceeds in two different ways. At a photon energy of 50 eV, double ionization from the ground state occurs through the absorption of two photons in the K shell, resulting in ionization of a single $1s$ electron, followed by ionization of the $2s$ valence electron via an $(e,2e)$ collision process during the ejection of the $1s$ electron, or via a "shake-off' process in which the $1s$ electron is ejected so rapidly that the residual ion does not have sufficient time to adjust adiabatically to the Li^+ ground state, and the second electron relaxes to a state which is in the continuum. At a photon energy of 59 eV, the absorption of a single photon resonantly excites the $1s2s2p$ doubly excited state. The absorption of a second photon is then sufficient to eject the $2s$ and $2p$ electrons. At this photon energy, we model only the second step of this process, namely, double photoionization of the $2s2p\ ^2P_{M=0}$ two-electron state. We make a comparison between the angular distributions of the two electrons emitted from the ground and doubly excited states, and also between the angular distributions of Li and He for a common LS symmetry. Such comparison provides information on the interaction of VUV light with electrons from different n shells.

II. THEORY

A. Time-dependent close-coupling method

The time-dependent close-coupling (TDCC) method employed in this work is capable of treating single, double, and triple photoionization of a three-electron system in full dimensionality [33–36]. However, the current work focuses on double ionization, and so the lithium atom is treated as a two-active-electron system [37], where the inner $1s$ electron is considered to be inactive. The two-electron wave function for a given spin S is given as an expansion on a basis set of coupled spherical harmonics, $|l_1 l_2 L\rangle$, of the form

$$\Psi^S(\mathbf{r}_1,\mathbf{r}_2,t) = \sum_{l_1,l_2,L} \frac{P^{LS}_{l_1l_2}(r_1,r_2,t)}{r_1 r_2} |l_1 l_2 L\rangle. \tag{1}$$

In this work, we employ two different approaches to solving the full-dimensional two-electron time-dependent Schrödinger equation. For two-photon double ionization, the above expansion may be used to obtain the set of time-dependent close-coupling equations for each LS term, given by

$$\begin{aligned} i\frac{\partial}{\partial t} P^{LS}_{l_1l_2}(r_1,r_2,t) &= T_{l_1l_2}(r_1,r_2) P^{LS}_{l_1l_2}(r_1,r_2,t) \\ &+ \sum_{l_1',l_2'} V^{L}_{l_1l_2,l_1'l_2'}(r_1,r_2) P^{LS}_{l_1'l_2'}(r_1,r_2,t) \\ &+ \sum_{l_1',l_2',L'} W^{LL'}_{l_1l_2,l_1'l_2'}(r_1,r_2,t) P^{L'S}_{l_1'l_2'}(r_1,r_2,t). \end{aligned} \tag{2}$$

In Eq.(2), $T_{l_1l_2}(r_1,r_2)$ is the atomic Hamiltonian, given by

$$\begin{aligned} &T_{l_1l_2}(r_1,r_2) \\ &= \sum_{j=1}^{2} \left[-\frac{1}{2}\frac{\partial^2}{\partial r_j^2} - \frac{Z}{r_j} + \frac{l_j(l_j+1)}{2r_j^2} + V_D(r_j) + V_X(r_j) \right], \end{aligned} \tag{3}$$

where the "direct" potential term $V_D(r_j)$ is defined in terms of a hydrogenic ground-state radial orbital of Li^{2+}, $P_{1s}(r')$,

$$V_D(r) = \int_0^\infty \frac{P^2_{1s}(r')}{\max(r',r)} dr', \tag{4}$$

and the "exchange" potential term $V_X(r_j)$ is calculated using a semiempirical local potential

$$V_X(r) = -\alpha \left(\frac{24\rho_{1s}(r)}{\pi} \right)^{1/3}, \tag{5}$$

where α is an adjustable parameter, which may be varied in order to obtain energy levels close to those of experiment. We found that a value of $\alpha = 0.3487$ gave reasonable energies for the ground and first few singly excited states of Li^+. The parameter $\rho_{1s}(r) = P^2_{1s}(r)/4\pi r^2$ is the radial probability density of the core electron. The two-electron terms $V^{L}_{l_1l_2,l_1'l_2'}(r_1,r_2)$ and $W^{LL'}_{l_1l_2,l_1'l_2'}(r_1,r_2,t)$ are the dielectronic repulsion and radiation field operators, respectively. This approach gives a reasonable treatment of the interaction of the inactive $1s$ electron with the outgoing electrons, and has been used recently in studies of electron-impact single ionization of He [38] and double photoionization of Li [39].

For single-photon double ionization, we solve the set of "weak-field" close-coupling equations, given by

$$\begin{aligned} i\frac{\partial}{\partial t} P^{LS}_{l_1l_2}(r_1,r_2,t) &= T_{l_1l_2}(r_1,r_2) P^{LS}_{l_1l_2}(r_1,r_2,t) \\ &+ \sum_{l_1',l_2'} V^{L}_{l_1l_2,l_1'l_2'}(r_1,r_2) P^{LS}_{l_1'l_2'}(r_1,r_2,t) \\ &+ \sum_{l_1',l_2'} W^{LL_0}_{l_1l_2,l_1'l_2'}(r_1,r_2) e^{-iE_0t} P^{L_0S}_{l_1'l_2'}(r_1,r_2), \end{aligned} \tag{6}$$

where $P^{L_0S}_{l_1'l_2'}(r_1,r_2)$ is the initial state wave function for a given value of L_0, E_0 is the initial state energy, and all other terms are defined as in Eq. (2). The two-electron wave function for the initial state is obtained through solution of the two-electron time-dependent Schrödinger equation in imaginary time. This is straightforward for the $1s2s\ ^3S$ two-electron state, which is the lowest possible state for this symmetry. However, since the lowest possible ^1S two-electron state is $1s^2$, a Schmidt orthogonalization of the $1s2s\ ^1S$ state to the $1s^2\ ^1S$ state must be performed, to avoid relaxation to an unphysical $1s^3$ three-electron state of Li. When relaxing to the $2s2p\ ^{1,3}P$ two-electron states, a similar orthogonalization procedure is required to avoid relaxation to a state involving $1s$ character. Typically, a relaxation time of 20 atomic units (0.5 fs) is sufficient to ensure that spurious contributions from highly excited states are removed. The resulting double ionization threshold for the $1s^22s\ ^2S$ state is found to be 82.6 eV, within 2% of the exact value of 81.03 eV [40]. For the $1s2s2p\ ^2P$ state, the double ionization threshold is found to be 22.3 eV, within 1% of the exact value of 22.12 eV [40].

Calculations pertaining to two-photon double ionization of the Li ground state were performed on basis sets containing 15 coupled channels in the initial $^{1,3}S$ states. The set of $^{1,3}S$, $^{1,3}P$, and $^{1,3}D$ final states consisted of 83 coupled channels, with $0 \leqslant l_1,l_2 \leqslant 14$. The large range of angular momenta was required for accurate description of the diffuse $2s$ orbital. At high laser intensities, $^{1,3}F$ states were included in the calculations for convergence purposes, resulting in a total of 123 coupled channels for the same range of l_1 and l_2. Calculations pertaining to photoionization of the Li $1s2s2p$ doubly excited state required basis sets containing 28 coupled channels in the initial $^{1,3}P$ states. The set of $^{1,3}S$ and $^{1,3}D$ final states consisted of 55 coupled channels, with $0 \leqslant l_1,l_2 \leqslant 14$. A finite-difference radial grid consisting of $(960)^2$ points with uniform mesh spacing $\delta r = 0.1$ a.u. was used for the radial wave functions in both sets of calculations. The use of a radial grid extending to 120 a.u. did not alter the results in any significant way.

Following the time propagation of Eq. (1), at a final time $t = T$, the final state radial wave functions $P^{LS}_{l_1l_2}(r_1,r_2,T)$ are projected onto fully antisymmetric products of normalized Li^{2+} continuum orbitals to obtain final state momentum-space wave functions $\mathcal{P}^{LS}_{l_1l_2}(k_1,k_2,T)$, so that

$$\begin{aligned} &\mathcal{P}^{LS}_{l_1l_2}(k_1,k_2,T) \\ &= \int_0^\infty dr_1 \int_0^\infty dr_2\ P_{k_1l_1}(r_1) P_{k_2l_2}(r_2) P^{LS}_{l_1l_2}(r_1,r_2,T), \end{aligned} \tag{7}$$

where the $P_{kl}(r)$ are the normalized Li^{2+} continuum orbitals, obtained through solution of the field-free radial one-electron time-independent Schrödinger equation using the direct and exchange potentials defined earlier.

To obtain angular distributions for two ionizing electrons, triple differential cross sections may be calculated for both two-photon double ionization of the Li $1s^2 2s\,^2S$ state and photoionization of the Li $1s2s2p\,^2P$ state. The triple differential cross section (TDCS) for two-photon double ionization is given by [13]

$$\frac{d^3\sigma}{dE_1\,d\Omega_1\,d\Omega_2} = 2\frac{1}{k_1k_2}\left(\frac{\omega}{I}\right)^2\frac{1}{T_{\rm eff}}\int_0^\infty dk_1\int_0^\infty dk_2\,\delta\left[\alpha-\tan^{-1}\left(\frac{k_2}{k_1}\right)\right] \times\sum_S w_S\left|\sum_{l_1,l_2,L}(-i)^{l_1+l_2}e^{i(\delta_{l_1}+\delta_{l_2}+\eta_{l_1}+\eta_{l_2})}\mathcal{P}^{LS}_{l_1l_2}(k_1,k_2,T)|l_1l_2L\rangle\right|^2, \tag{8}$$

where the initial factor of 2 arises from the initial double occupation of the $1s$ orbital, ω is the photon energy, I is the laser intensity, $T_{\rm eff}$ is the effective pulse duration, given by the integration of the applied pulse envelope, and α is the hyperspherical angle between k_1 and k_2. The spin-dependent terms w_S are the appropriate spin statistical factors for the singlet and triplet state contributions, namely, $w_0 = 1/4$ and $w_1 = 3/4$, δ_{l_1} and δ_{l_2} are scattered phase shifts, η_{l_1} and η_{l_2} are distorted-wave phase shifts, and $|l_1l_2L\rangle$ are momentum-space coupled spherical harmonics. For single-photon double ionization of the $2s2p\,^{1,3}P$ two-electron states, the TDCS takes the form [32]

$$\frac{d^3\sigma}{dE_1\,d\Omega_1\,d\Omega_2} = \frac{1}{k_1k_2}\frac{\omega}{I}\frac{\partial}{\partial t}\int_0^\infty dk_1\int_0^\infty dk_2\,\delta\left[\alpha-\tan^{-1}\left(\frac{k_2}{k_1}\right)\right] \times\sum_S w_S\left|\sum_{l_1,l_2,L}(-i)^{l_1+l_2}e^{i(\delta_{l_1}+\delta_{l_2}+\eta_{l_1}+\eta_{l_2})}\mathcal{P}^{LS}_{l_1l_2}(k_1,k_2,T)|l_1l_2L\rangle\right|^2, \tag{9}$$

where all quantities are defined as in the TDCS for two-photon double ionization. The differences in the time-dependent terms of the two TDCS expressions (8) and (9) are due to the different treatments of the temporal evolution of the laser-atom interactions in the close-coupling equations (2) and (6).

III. RESULTS

A. Two-photon double ionization of the Li $1s^2 2s\,^2S$ ground state

Figure 1 shows the TDCS for equal energy sharing from an initial $1s2s\,^1S$ two-electron state, with the two electrons being ejected at polar angles θ_1 and θ_2, at a photon energy of 50 eV and a laser intensity of 5×10^{14} W/cm^2. The TDCS is calculated in coplanar geometry ($\phi_1 = \phi_2 = 0^\circ$), and is plotted as a function of polar angle θ_2 for a number of values of θ_1. Both θ_1 and θ_2 are measured relative to the laser polarization axis. For $\theta_1 = 0^\circ$, the TDCS displays a strong

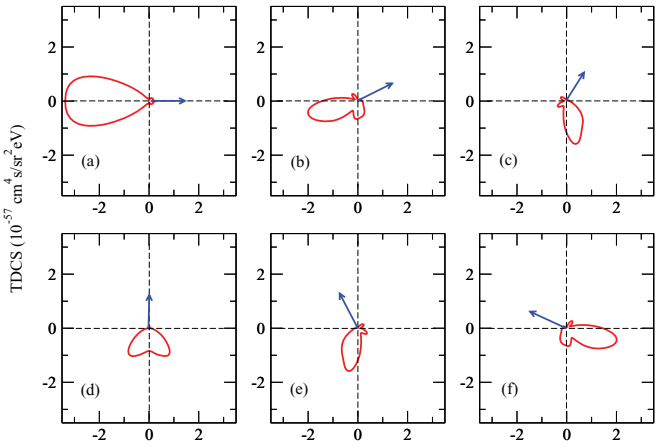

FIG. 1. (Color online) Triple differential cross sections for two-photon double ionization from the $1s2s\,^1S$ two-electron state of Li, for equal energy sharing and various double-ejection configurations. The results are plotted as a function of polar angle θ_2 for (a) $\theta_1 = 0^\circ$, (b) $\theta_1 = 30^\circ$, (c) $\theta_1 = 60^\circ$, (d) $\theta_1 = 90^\circ$, (e) $\theta_1 = 120^\circ$, and (f) $\theta_1 = 150^\circ$. The photon energy is 50 eV and the laser intensity is 5×10^{14} W/cm^2. The arrows indicate the angle of escape of electron 1.

peak at $\theta_2 = 180^\circ$, indicating dominant antiparallel emission of the two electrons into opposite spatial hemispheres, induced by the Coulomb repulsion. This contrasts with the electron dynamics of single-photon double ionization of the Li ground state, where antiparallel emission is forbidden by the dipole selection rules for equal energy sharing [41]. For other values of θ_1 there is generally one large peak and two smaller peaks, except for $\theta_1 = 90^\circ$, where there are two peaks at $\theta_2 = \theta_1 \pm 135^\circ$. It is informative to make a comparison between the dominant double-ejection configurations arising from two-photon double ionization of the $1s2s\,^1S$ two-electron state of Li and those occurring in two-photon double ionization of the He $1s^2\,^1S$ ground state at a photon energy of 42 eV [16]. For $\theta_1 = 0^\circ$, both He and Li have a single large peak at $\theta_2 = 180^\circ$. For $\theta_1 = 30^\circ$ and $\theta_1 = 150^\circ$, the TDCS for both He and Li is dominated by antiparallel emission, with an additional contribution from emission of two electrons perpendicular to each other. For $\theta_1 = 60^\circ$ and $\theta_1 = 120^\circ$, the TDCS for both He and Li has a peak close to perpendicular emission, however, He has large peaks at $\theta_1 = 60^\circ$,$\theta_2 = 200^\circ$ and $\theta_1 = 120^\circ$,$\theta_2 = 340^\circ$. For Li, these peaks are also present, but make a smaller relative contribution compared to the corresponding peak for He. At $\theta_1 = 90^\circ$, the second electron in He is predominantly emitted at $\theta_1 \pm 110^\circ$, whereas for Li the peaks are slightly shifted to $\theta_2 = \theta_1 \pm 135^\circ$, with a smaller additional contribution from antiparallel emission. The variation is most likely due to differences in the interference between the outgoing $1s$ and $2s$ electrons in Li, compared to the two $1s$ electrons in He. Differences in the relative contributions of the individual peaks in the TDCS may also be due to differences in the excess energy available to the outgoing electrons. A partial wave decomposition of the TDCS shows that final S states mainly contribute to antiparallel emission, whereas final D states make contributions at other angles, while also contributing to antiparallel emission. The same decomposition for two-photon double ionization of He

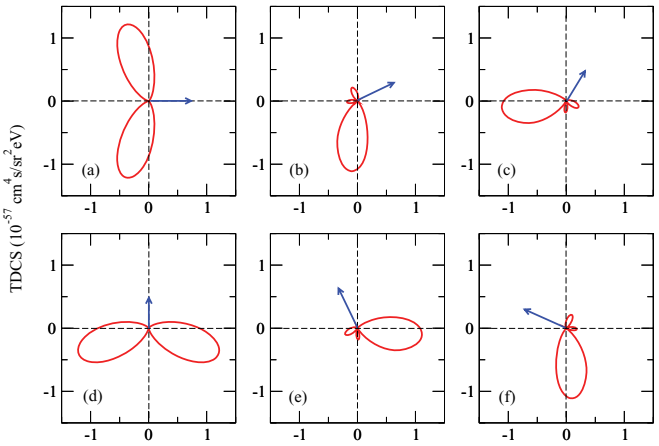

FIG. 2. (Color online) Triple differential cross sections for two-photon double ionization from the $1s2s\ ^3S$ two-electron state of Li, for equal energy sharing and various double-ejection configurations. The results are plotted as a function of polar angle θ_2 for (a) $\theta_1 = 0°$, (b) $\theta_1 = 30°$, (c) $\theta_1 = 60°$, (d) $\theta_1 = 90°$, (e) $\theta_1 = 120°$, and (f) $\theta_1 = 150°$. The photon energy is 50 eV and the laser intensity is 5×10^{14} W/cm^2. The arrows indicate the angle of escape of electron 1.

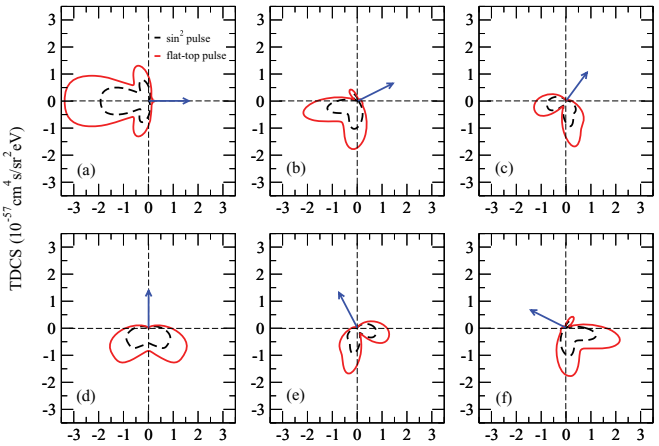

FIG. 3. (Color online) Variation in the total TDCS with laser pulse profile, for equal energy sharing and various double-ejection configurations. The results are plotted as a function of polar angle θ_2 for (a) $\theta_1 = 0°$, (b) $\theta_1 = 30°$, (c) $\theta_1 = 60°$, (d) $\theta_1 = 90°$, (e) $\theta_1 = 120°$, and (f) $\theta_1 = 150°$. The black dashed curve is the TDCS obtained using a ten-cycle sin^2 laser pulse profile. The red solid curve is the TDCS obtained using a ten-cycle flat-top pulse profile (see text for details). The photon energy is 50 eV and the laser intensity is 5×10^{14} W/cm^2. The arrows indicate the angle of escape of electron 1.

yielded similar features [16]. This behavior naturally reflects increasing contributions from the higher harmonics in the D partial waves. A similar comparison between the TDCS of He and H^- for a common excess energy (shared equally) has recently been presented in [31]. Many common features were found in the TDCS for two different two-electron atoms, and despite differences in the magnitude of the TDCS, a number of similar angular selection rules were observed in both He and H^-.

It is also clear in Fig. 1 that the magnitude of the TDCS is largest for $\theta_1 = 0°$. This indicates a preference for emission of the two electrons in opposite directions along the laser polarization axis, since antiparallel emission is dominant for this configuration. For other configurations, the magnitude of the TDCS is largely insensitive to the value of θ_1, except for $\theta_1 = 90°$, where the TDCS contains two peaks, and is smaller in magnitude than for other values of θ_1.

Figure 2 shows the TDCS for equal energy sharing from an initial $1s2s\ ^3S$ two-electron state for a range of double-ejection configurations at a photon energy of 50 eV and a laser intensity of 5×10^{14} W/cm^2. In contrast to the results shown in Fig. 1, antiparallel emission is now avoided for $\theta_1 = 0°$, with the dominant peaks in the TDCS appearing close to $\theta_2 = 120°$ and $\theta_2 = 240°$. This naturally contrasts with the selection rules observed in photoionization of the $1s2s\ ^3S$ state of helium [32] and lithium [39], where antiparallel emission is dominant. For other values of θ_1 there is usually a single large peak, except for $\theta_1 = 90°$, where two peaks appear at $\theta_2 = \theta_1 \pm 120°$. It is also apparent that the magnitude of the TDCS is approximately equal for $\theta_1 = 0°$ and $\theta_1 = 90°$. This contrasts with the TDCS for the ^1S state, where there was a preference for emission along the laser polarization axis. For the ^3S state, the TDCS for $\theta_1 = 0°$ and $\theta_1 = 90°$ has two large peaks of equal magnitude, and for other configurations has a single peak whose magnitude is largely insensitive to the value of θ_1. In this case, a partial wave decomposition shows that final S states make a negligible contribution to the TDCS at all values of θ_1. This contrasts strongly with the singlet case, where final S and D waves often make contributions of similar magnitudes.

It is instructive to examine the variation in the TDCS with laser pulse profile. In Figs. 1 and 2, the TDCS is calculated using a ten-cycle flat-top laser pulse, consisting of a single cycle ramp-on and ramp-off, and eight laser cycles at peak intensity. To examine the effect of laser pulse profile on the TDCS, we also calculate the TDCS using a ten-cycle sin^2 laser pulse profile. In both cases, an additional two laser cycles of field-free propagation are allowed after the laser pulse has ramped off, so that a stable solution may be reached. In Fig. 3, we show the total (singlet and triplet contributions combined) TDCS for these two different pulse shapes. It is clear that the selection rules are not affected by the laser pulse shape, although the magnitude of the TDCS does vary. This difference may be attributed to the differing "average" intensities experienced by the two electrons. By considering the integral of each laser pulse profile, we find that the average intensity of the flat-top pulse is 1.8 times larger than that of the sin^2 pulse. Consequently, the TDCS obtained using a flat-top pulse shape is 1.8 times larger than that obtained using a sin^2 pulse shape.

We also investigate the variation in the TDCS as a function of laser intensity. In Fig. 4, we show the TDCS for equal energy sharing and various double-ejection configurations obtained at two different laser intensities: 5×10^{14} W/cm^2 and 1×10^{15} W/cm^2. We find that neither the magnitude nor the angular selection rules are sensitive to laser intensities in this range.

Figure 5 shows variation in the TDCS for both initial singlet and triplet $1s2s$ two-electron states with the escape energy of electron 2, for $\theta_1 = 0°$ and $\theta_1 = 90°$. The angular distributions for $E_1 = 15$ eV and $E_2 = 3$ eV, $E_1 = 13$ eV and $E_2 = 5$ eV,

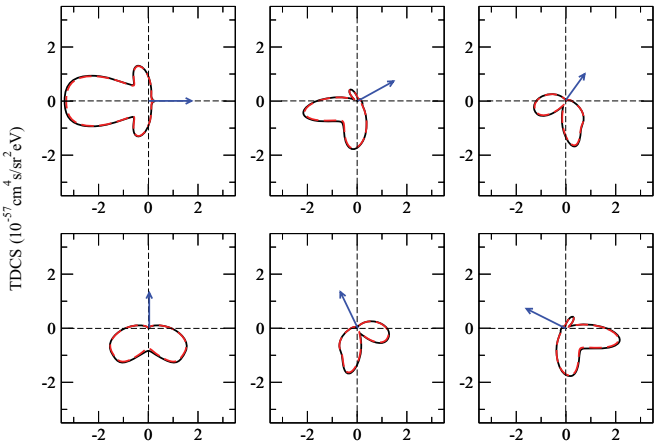

FIG. 4. (Color online) Variation in the total TDCS with laser intensity, for equal energy sharing and various double-ejection configurations. The black solid curve is the TDCS obtained using a laser intensity $I = 5 \times 10^{14}$ W/cm^2. The red dashed curve is the TDCS obtained using a laser intensity $I = 1 \times 10^{15}$ W/cm^2. The arrows indicate the angle of escape of electron 1.

and $E_1 = E_2 = 9$ eV are shown from left to right. For $\theta_1 = 0^\circ$, antiparallel emission dominates for an initial singlet state, regardless of how the excess energy is shared between the two electrons. For an initial triplet state, antiparallel emission dominates for $E_2 = 3$ eV, but is then avoided in the case of equal energy sharing.

For $\theta_1 = 90^\circ$, antiparallel emission is no longer dominant for an initial triplet state with unequal energy sharing. Instead, the electrons generally depart at $\pm 120^\circ$ to each other regardless of how the excess energy is shared. For an initial singlet state, antiparallel emission dominates for $E_2 = 3$ eV and $\theta_1 = 90^\circ$, but becomes progressively less prominent as E_2 increases. It is also notable that, for $\theta_1 = 90^\circ$, the magnitude of the TDCS for both the singlet and triplet states increases

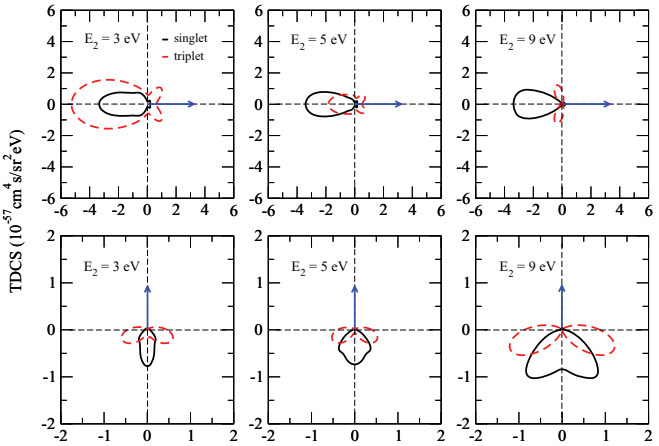

FIG. 5. (Color online) TDCS for both initial singlet and triplet $1s2s$ two-electron states for different energy sharing for $\theta_1 = 0^\circ$ (top panels) and $\theta_1 = 90^\circ$ (bottom panels). The escape energy of electron 2, E_2, is indicated in each panel. The case $E_2 = 9$ eV corresponds to equal energy sharing. The photon energy is 50 eV and the laser intensity is 5×10^{14} W/cm^2. Note the change of scale in the lower panels.

as E_2 approaches E_1. This behavior is not seen for $\theta_1 = 0^\circ$, where the magnitude of the TDCS decreases noticeably for the triplet state, and decreases more slowly for the singlet state. We find that the magnitude of the TDCS for the singlet state with $\theta_1 = 0^\circ$ increases more noticeably when $E_2 < 1$ eV. A preference for ejection of two electrons with unequal energies indicates that double ionization occurs due to a shake-off process. In this process, a single electron absorbs both photons, and is ejected with a high energy. The ejection of the first electron is so rapid that the second electron experiences a strongly modified ionic potential, and can only relax to a state which may be in the continuum. A preference for ejection of both electrons with similar energies suggests that double ionization is mediated by a "knock-out" process, where a single electron is ionized after absorbing both photons, and, during its escape, ejects the second electron in an $(e,2e)$ collision. The results shown in Fig. 5 suggest that at $\theta_1 = 0^\circ$, double ionization is predominantly caused by shake off, whereas at $\theta_1 = 90^\circ$, a knock-out mechanism becomes more prominent. We cannot quantify the relative contributions of these competing mechanisms, which may also interfere, although it is to be expected that the most energetic electrons should be those that receive the greatest assistance from the laser field (i.e., those ejected along the laser polarization axis). The rapid escape of these energetic electrons should then induce ionization of the remaining electron via shake off. Consequently, when one electron is ejected away from the laser polarization axis, an $(e,2e)$ collision process ought to make an increased contribution to the double ionization mechanism.

It is also apparent that although the magnitude of the TDCS for the triplet state remains approximately constant for $\theta_1 = 0^\circ$ and $\theta_1 = 90^\circ$ at equal energy sharing, this is not the case for unequal energy sharing. In fact, the triplet state manifests a strong preference for ejection of both electrons in opposite directions along the laser polarization axis (as is the case for the singlet state), but only when the excess energy is not shared equally. Such dependence on the energy sharing is often seen in double photoionization, where certain double-ejection configurations are forbidden by selection rules when the excess energy is shared equally, but are allowed when the excess energy is not shared equally.

B. Single-photon double ionization of the Li $1s2s2p\,^2P$ state

Figure 6 shows the TDCS for equal energy sharing from an initial $2s2p\ ^1P$ two-electron state for a range of double-ejection configurations at a photon energy of 59 eV and a laser intensity of 5×10^{14} W/cm^2. The TDCS is again calculated in coplanar geometry ($\phi_1 = \phi_2 = 0^\circ$), and is plotted as a function of polar angle θ_2 for a number of values of θ_1. For $\theta_1 = 0^\circ$, the TDCS displays a strong peak at $\theta_2 = 180^\circ$, as was the case for an initial $1s2s\ ^1S$ two-electron state. However, at other values of θ_1 the TDCS takes a very different form from that obtained using an initial $1s2s$ state. For $\theta_1 = 30^\circ$ and $\theta_1 = 150^\circ$, perpendicular emission is now favored over antiparallel emission (which was dominant in the $1s2s$ state). Moreover, perpendicular emission either side of the laser polarization axis is favored at all values of θ_1, as a means of conserving the momentum components perpendicular to the polarization vector. For $\theta_1 = 60^\circ$ and $\theta_1 = 120^\circ$, the TDCS

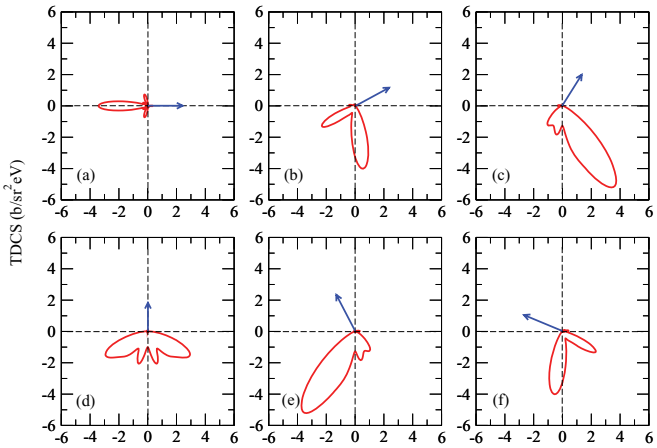

FIG. 6. (Color online) Triple differential cross sections for double photoionization from the $2s2p\,^1P$ two-electron state of Li, for equal energy sharing and various double-ejection configurations. The results are plotted as a function of polar angle θ_2 for (a) $\theta_1 = 0°$, (b) $\theta_1 = 30°$, (c) $\theta_1 = 60°$, (d) $\theta_1 = 90°$, (e) $\theta_1 = 120°$, and (f) $\theta_1 = 150°$. The photon energy is 59 eV and the laser intensity is 5×10^{14} W/cm^2. The arrows indicate the angle of escape of electron 1.

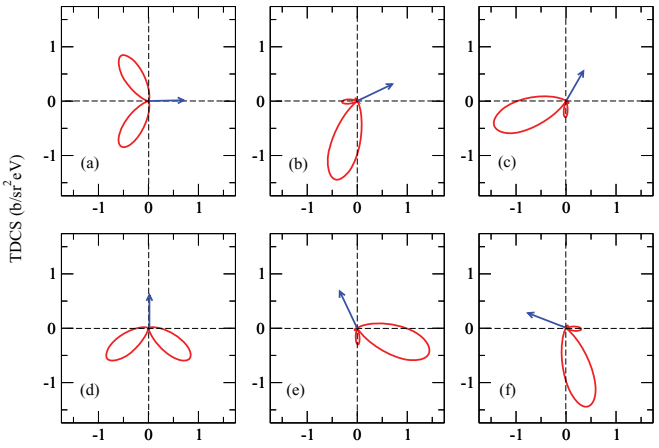

FIG. 7. (Color online) Triple differential cross sections for double photoionization from the $2s2p\,^3P$ two-electron state of Li, for equal energy sharing and various double-ejection configurations. The results are plotted as a function of polar angle θ_2 for (a) $\theta_1 = 0°$, (b) $\theta_1 = 30°$, (c) $\theta_1 = 60°$, (d) $\theta_1 = 90°$, (e) $\theta_1 = 120°$, and (f) $\theta_1 = 150°$. The photon energy is 59 eV and the laser intensity is 5×10^{14} W/cm^2. The arrows indicate the angle of escape of electron 1.

is more similar to its $1s2s$ counterpart, with perpendicular emission favored over a much smaller contribution from antiparallel emission. For $\theta_1 = 90°$, the electrons are primarily ejected at approximately 120° to one another, with secondary contributions from $\theta_2 = \theta_1 \pm 160°$. As before, a partial wave decomposition of the TDCS shows that final S states mainly contribute to antiparallel emission, whereas final D states are responsible for the structures at other values of θ_2. In contrast to the variation in the TDCS observed for the $1s2s\,^1S$ state, the TDCS for the $2s2p\,^1P$ state now increases as θ_1 is varied from 0° to 60°. This behavior indicates a preference for emission of two electrons away from the laser polarization axis when the electrons are emitted with equal energies. Such a preference has previously been seen for equal energy sharing in photoionization of the $2s2p^1P$ two-electron excited state of Be [42].

Figure 7 shows the TDCS for equal energy sharing from an initial $2s2p\,^3P$ two-electron state for a range of double-ejection configurations at a photon energy of 59 eV and a laser intensity of 5×10^{14} W/cm^2. In this case, the selection rules of the angular distribution for each value of θ_1 appear similar to their $1s2s$ counterparts. For $\theta_1 = 0°$ and $\theta_1 = 90°$, there are two strong peaks at $\theta_2 = \theta_1 \pm 120°$. For other values of θ_1 there is a single large peak, which is slightly shifted in comparison to its $1s2s\,^3S$ counterpart. It is also noticeable that the magnitude of the TDCS is at its smallest for $\theta_1 = 0°$. This behavior was also observed in the TDCS for equal energy sharing in photoionization of the $2s2p\,^3P$ two-electron state of Be [42]. Many of the features of the TDCS are confirmed by the selection rules for double photoionization listed in [41]. For example, selection rule C in [41] dictates that, for equal energy sharing, the TDCS for a triplet final state of even parity must contain no contribution from antiparallel emission. This is most clearly seen for $\theta_1 = 0°$ and $\theta_1 = 90°$, but can also be seen between the main lobe features at all other values of θ_1. Selection rule D in [41] also dictates that the TDCS in this case must be zero for $\theta_1 = \theta_2$ with equal energy sharing. Furthermore, selection rules F and H dictate that the TDCS should be zero for $\theta_2 = \pi - \theta_1$. For $\theta_1 = 0°$, this naturally follows from selection rule C, but for other values of θ_1, such a zero is visible between the two smaller lobe features for $\theta_1 = 30°$ and $\theta_1 = 150°$, and can be more clearly seen for $\theta_1 = 60°$, 90°, and 120°. As for two-photon double ionization of the $1s2s\,^3S$ state, a partial wave decomposition of the TDCS shows that final S states make a negligible contribution for all values of θ_1. This result confirms selection rule E in [41], which states that final $^3S^e$ states make no contribution to the TDCS in the case of equal energy sharing.

Finally, Fig. 8 shows variation in the TDCS for both singlet and triplet initial states with the escape energy of each electron for $\theta_1 = 0°$ and $\theta_1 = 90°$. For $\theta_1 = 0°$, the TDCS for the initial

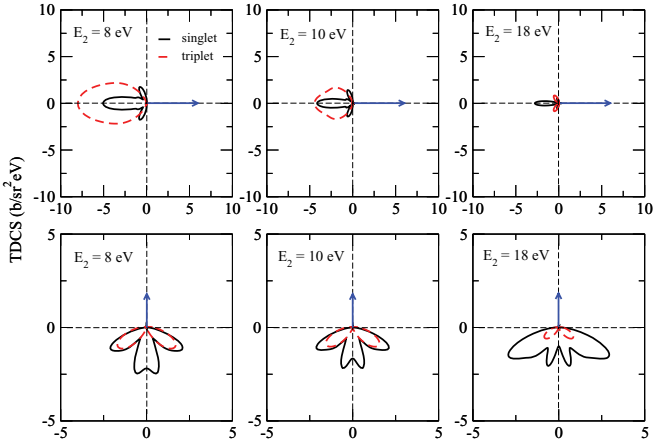

FIG. 8. (Color online) Variation in the triple differential cross sections with energy sharing for $\theta_1 = 0°$ (top panels) and $\theta_1 = 90°$ (lower panels). The case $E_2 = 18$ eV corresponds to equal energy sharing. The photon energy is 59 eV and the laser intensity is 5×10^{14} W/cm^2. The arrows indicate the angle of escape of electron 1. Note the change of scale in the lower panels.

$2s2p\ ^1P$ state varies in magnitude as the E_1 increases, although the selection rules are unaltered. However, the initial ^3P state shows a very different behavior, displaying a large variation in the selection rules. For $E_1 = 8$ eV, antiparallel emission is dominant, as it is for the ^1P state. However, the maximum in the TDCS gradually decreases as E_1 increases, and becomes a minimum when $E_1 = E_2$. Conversely, when $\theta_1 = 90^\circ$, the selection rules of the ^3P state do not vary with electron energy, but those of the ^1P state vary strongly. For $E_1 =$ 8 eV, antiparallel emission is dominant in the ^1P state, with additional contributions from $\theta_2 = 210^\circ$ and $\theta_2 = 330^\circ$. As E_1 increases, the additional components increase in magnitude, whereas antiparallel emission becomes less prevalent. All of these trends are very similar to those observed for two-photon double ionization of the $1s2s\ ^{1,3}S$ states.

However, it is clear that the variation in the magnitude of the TDCS with electron energy sharing is different from that observed in Fig. 5. In particular, the singlet state now demonstrates a more visible preference for ejection at unequal energies than was the case for the $1s2s\,^1S$ state. Additionally, for $\theta_1 = 90^\circ$ the magnitude of the TDCS for both singlet and triplet states decreases as E_2 increases. This behavior indicates that double ionization is predominantly induced by a shake-off mechanism. The increasing contribution of the shake-off mechanism as photon energy is increased has previously been observed for He [16].

IV. SUMMARY

In summary, we have presented the first calculations of the angular distributions for two-photon double ionization of lithium. We have considered two different double-ionization pathways: first, direct two-photon double ionization from the ground state, and secondly, photoexcitation of the $1s2s2p\ ^2P$ doubly excited state followed by double photoionization. We have discussed the main features of the angular distributions, and the main similarities and differences in the competing double-ionization geometries for these two different processes. We also make a comparison between the angular distributions obtained for two-photon double ionization of the $1s2s\ ^1S$ state of lithium with those of the helium $1s^2\ ^1S$ ground state. Again, the comparison reveals a number of common double-ejection configurations, although new features do appear in the distributions for Li which are not seen for He. These differences may shed some light on the interaction of two electrons emitted from different shells with the laser field. Future theoretical exploration of such effects will be essential to complement ongoing experimental studies of two-photon double ionization of multielectron atoms.

Additionally, we have investigated the sensitivity of the angular distributions to laser pulse profile and intensity. We observe little variation in the distributions as the laser intensity is varied by a factor of 2. However, the magnitude of the distributions is sensitive to the laser pulse profile, which determines the mean laser intensity experienced by the atom. Nevertheless, the double-ejection configurations remain the same regardless of the laser pulse profile. It is hoped that current and future experiments will be able to provide an experimental check of the results presented in this work.

ACKNOWLEDGMENTS

The Los Alamos National Laboratory is operated by Los Alamos National Security, LLC for the National Nuclear Security Administration of the US Department of Energy under Contract No. DE-AC5206NA25396. Computational work was carried out at Los Alamos National Laboratory through the provision of an Institutional Computing award. We thank A. S. Kheifets, A. Dorn and M. S. Pindzola for useful discussions.

[1] A. Rudenko *et al.*, Phys. Rev. Lett. **101**, 073003 (2008).
[2] M. Kurka *et al.*, J. Phys. B: At. Mol. Opt. Phys. **43**, 194004 (2010).
[3] M. Kurka *et al.*, New J. Phys. **12**, 073035 (2010).
[4] G. Zhu, M. Schuricke, J. Steinmann, J. Albrecht, J. Ullrich, I. Ben-Itzhak, T. J. M. Zouros, J. Colgan, M. S. Pindzola, and A. Dorn, Phys. Rev. Lett. **103**, 103008 (2009).
[5] M. Schuricke, G. Zhu, J. Steinmann, K. Simeonidis, I. Ivanov, A. Kheifets, A. N. Grum-Grzhimailo, K. Bartschat, A. Dorn, and J. Ullrich, Phys. Rev. A **83**, 023413 (2011).
[6] L. Hamonou, H. W. van der Hart, K. M. Dunseath, and M. Terao-Dunseath, J. Phys. B: At. Mol. Opt. Phys. **41**, 015603 (2007).
[7] L. Hamonou and H. W. van der Hart, J. Phys. B: At. Mol. Opt. Phys. **41**, 121001 (2008).
[8] H. W. van der Hart, Phys. Rev. Lett. **95**, 153001 (2005).
[9] V. Richardson *et al.*, Phys. Rev. Lett. **105**, 013001 (2010).
[10] S. Fritzsche, A. N. Grum-Grzhimailo, E. V. Gryzolva, and N. M. Kabachnik, J. Phys. B: At. Mol. Opt. Phys. **44**, 175602 (2011).
[11] M. S. Pindzola and F. Robicheaux, J. Phys. B: At. Mol. Opt. Phys. **31**, L823 (1998).
[12] L. A. A. Nikolopoulos and P. Lambropoulos, J. Phys. B: At. Mol. Opt. Phys. **34**, 545 (2001).
[13] J. Colgan and M. S. Pindzola, Phys. Rev. Lett. **88**, 173002 (2002).
[14] L. Feng and H. W. van der Hart, J. Phys. B: At. Mol. Opt. Phys. **36**, L1 (2003).
[15] B. Piraux, J. Bauer, S. Laulan, and H. Bachau, Eur. J. Phys. D **26**, 7 (2003).
[16] S. X. Hu, J. Colgan, and L. A. Collins, J. Phys. B: At. Mol. Opt. Phys. **38**, L35 (2004).
[17] I. A. Ivanov and A. S. Kheifets, Phys. Rev. A **75**, 033411 (2007).
[18] L. A. A. Nikolopoulos and P. Lambropoulos, J. Phys. B: At. Mol. Opt. Phys. **40**, 1347 (2007).
[19] D. A. Horner, F. Morales, T. N. Rescigno, F. Martín, and C. W. McCurdy, Phys. Rev. A **76**, 030701 (2007).
[20] E. Foumouo, Ph. Antoine, L. Malegat, H. Bachau, and R. Shakeshaft, J. Phys. B: At. Mol. Opt. Phys. **41**, 051001 (2008).
[21] J. Feist, S. Nagele, R. Pazourek, E. Persson, B. I. Schneider, L. A. Collins, and J. Burgdörfer, Phys. Rev. A **77**, 043420 (2008).
[22] X. Guan, K. Bartschat, and B. I. Schneider, Phys. Rev. A **77**, 043421 (2008).

[23] D. A. Horner, C. W. McCurdy, and T. N. Rescigno, Phys. Rev. A **78**, 043416 (2008).
[24] R. Nepstad, T. Birkeland, and M. Førre, Phys. Rev. A **81**, 063402 (2010).
[25] H. Hasegawa, E. J. Takahashi, Y. Nabekawa, K. L. Ishikawa, and K. Midorikawa, Phys. Rev. A **71**, 023407 (2005).
[26] A. A. Sorokin, M. Wellhöfer, S. V. Bobashev, K. Tiedtke, and M. Richter, Phys. Rev. A **75**, 051402 (2007).
[27] J. Colgan, M. S. Pindzola, and F. Robicheaux, J. Phys. B: At. Mol. Opt. Phys. **41**, 121002 (2008).
[28] F. Morales, F. Martín, D. A. Horner, T. N. Rescigno, and C. W. McCurdy, J. Phys. B: At. Mol. Opt. Phys. **42**, 134013 (2009).
[29] X. Guan, K. Bartschat, and B. I. Schneider, Phys. Rev. A **82**, 041404 (2010).
[30] X. Guan, K. Bartschat, and B. I. Schneider, Phys. Rev. A **84**, 033403 (2011).
[31] R. Nepstad and M. Førre, Phys. Rev. A **84**, 021402 (2011).
[32] J. Colgan and M. S. Pindzola, Phys. Rev. A **67**, 012711 (2003).
[33] J. Colgan, M. S. Pindzola, and F. Robicheaux, Phys. Rev. Lett. **93**, 053201 (2004).
[34] J. Colgan, M. S. Pindzola, and F. Robicheaux, Phys. Rev. A **72**, 022727 (2005).
[35] J. Colgan and M. S. Pindzola, J. Phys. B: At. Mol. Opt. Phys. **39**, 1879 (2006).
[36] J. Colgan and M. S. Pindzola, Phys. Rev. Lett. **108**, 053001 (2012).
[37] J. Colgan, D. C. Griffin, C. P. Ballance, and M. S. Pindzola, Phys. Rev. A **80**, 063414 (2009).
[38] J. Colgan, O. Al-Hagan, D. H. Madison, A. J. Murray, and M. S. Pindzola, J. Phys. B: At. Mol. Opt. Phys. **42**, 171001 (2009).
[39] A. S. Kheifets, D. V. Fursa, I. Bray, J. Colgan, and M. S. Pindzola, Phys. Rev. A **82**, 023403 (2010).
[40] See http://physics.nist.gov/PhysRefData/ASD.
[41] F. Maulbetsch and J. S. Briggs, J. Phys. B: At. Mol. Opt. Phys. **28**, 551 (1995).
[42] F. L. Yip, C. W. McCurdy, and T. N. Rescigno, Phys. Rev. A **81**, 063419 (2010).